Hybrid Image Deblurring by Fusing Edge and Power Spectrum Information

Tao Yue[1], Sunghyun Cho[2*], Jue Wang[2] and Qionghai Dai[1]

[1]Tsinghua University, China
[2]Adobe Research, USA

Abstract. Recent blind deconvolution methods rely on either salient edges or the power spectrum of the input image for estimating the blur kernel, but not both. In this work we show that the two methods are inherently complimentary to each other. Edge-based methods work well for images containing large salient structures, but fail on small-scale textures. Power-spectrum-based methods, on the contrary, are efficient on textural regions but not on structural edges. This observation inspires us to propose a hybrid approach that combines edge-based and power-spectrum-based priors for more robust deblurring. Given an input image, our method first derives a structure prediction that coincides with the edge-based priors, and then extracts dominant edges from it to eliminate the errors in computing the power-spectrum-based priors. These two priors are then integrated in a combined cost function for blur kernel estimation. Experimental results show that the proposed approach is more robust and achieves higher quality results than previous methods on both real world and synthetic examples.

1   Introduction

Blind image deblurring, i.e. estimating both the blur kernel and the latent sharp image from an observed blurry image is a significantly ill-posed problem. It has been extensively studied in recent years, and various image priors have been explored in recent approaches for alleviating the difficulty. The problem however remains unsolved. In particular, as we will show later, although each individual method performs well in certain situations, none of them can reliably produce good results in all cases.

Among recent deblurring approaches, edge-based methods and power-spectrum-based ones have shown impressive performance [1,2,3,4,5,6,7,8,9,10,11]. *Edge-based methods* recover the blur kernel mainly from salient image edges, assuming the blurry edges extracted from the input image correspond to sharp, step-like edges in the latent image. *Power-spectrum-based methods* make the white random distribution assumption on the gradient of the latent image, so that the kernel's power spectrum can be recovered from the blurred image in a closed form. Phase retrieval methods can then be applied to recover the final blur kernel from its power spectrum.

The underlying assumptions of both approaches however do not hold in some common situations. For instance, edge-based methods may fail on images where strong edges are lacking or difficult to extract and analyze. On the other hand, the power-spectrum-based methods can handle small-scale textures well, but may be negatively

---

* Sunghyun Cho is currently with Samsung Electronics.

affected by strong edges and tend to produce erroneous kernel components when they are abundant. Given that the failure modes of these two approaches are complimentary to each other, in order to achieve better robustness and a wider application range, we propose a hybrid method that simultaneously utilizes both the strong edges and the power spectrum information extracted from an input image for blur kernel estimation. Specifically, we detect and separate the input image into two components favored by each method, and develop an optimization process that takes into account both types of information for reliable blur kernel estimation. We conduct thorough experiments to show that the proposed method is indeed more robust and achieves higher quality results in general than previous approaches that use only one source of information.

The main contributions of the proposed approach include: (1) a modified blur kernel power spectrum estimation approach that eliminates the negative impact from structural image edges; and (2) a hybrid kernel estimation method that effectively integrates edge and power spectrum information.

1.1   Related work

Strong edges are important components in nature images, and have been heavily explored for image deblurring. Existing approaches either extract strong edges explicitly and use them for kernel estimation [1,2,3,4,5], or use them implicitly by incorporating them into regularization terms [6,7,8]. In explicit methods, Jia [1] recovers the blur kernel from transparency on blurry edges. Joshi *et al.* [2] utilize sub-pixel differences of Gaussian edge detectors to detect edges from blurry image and predict their sharp version. Cho and Lee [4] propose to use simple image filters to predict sharp edges in the latent image from blurry ones in the input for kernel estimation. This method is further improved by Xu and Jia [12] by using better edge prediction and selection methods. Zhong *et al.* [13] estimate 1D profiles of the kernel from edges and reconstruct the kernel by inverse Radon transform. More recently Sun *et al.* [9] improve Cho and Lee [4]'s method by predicting sharp edges using patch-based data driven methods. In implicit methods, Fergus *et al.* [14] use the heavy-tail prior of image gradients and marginalize the joint distribution over all possible sharp images. Shan *et al.* [6] use sparse priors to suppress insignificant structures for kernel estimation. Krishnan *et al.* [7] instead propose to use L_1/L_2 regularizer for edge selection. Recently, Xu *et al.* [8] propose to use L_0 sparse representation for the same purpose.

Power-spectrum-based methods try to recover the blur kernel directly from the input image without alternatively estimating the blur kernel and the latent sharp image, by using the fact that the gradients of natural images are approximately uncorrelated. Yitzhaky *et al.* [15] handle 1D motion blur by analyzing the characteristics of the power spectrum of the blurred image along the blur direction. Similarly Hu *et al.* [10] use an eight-point Laplacian whitening method to whiten the power spectrum of the image gradients and use it for estimating a 2D blur kernel. To deal with the irregularities of strong edges, Goldstein *et al.* [11] use a power-law model as well as a dedicated spectral whitening formula for achieving more robust kernel estimation.

For spectrum-based methods, phase retrieval is a key step to recover the blur kernel from the estimated power spectrum. It is a well studied problem in optical imaging field such as electron microscopy, wave front sensing, astronomy, crystallography,

etc. Fienup [16] compare the classical phase retrieval algorithms and report the stagnate problem of the existing algorithms. He and Wackerman [17] discuss the stagnate problem in detail and propose several solutions to overcome different kinds of stagnate. Luke [18] proposes a Relaxed Averaged Alternating Reflection (RAAR) algorithm which is later adopted by Goldstein and Fattal's approach [11]. Osherovich [19] recently proposes a method that achieves fast and accurate phase retrieval from a rough initialization.

2   Overview

2.1   Blur model

To model the camera shake in a blurred image, we use a conventional convolution based blur model:

$$b = k * l + n, \tag{1}$$

where b is a blurred image, k is a blur kernel, l is a latent image, and n is noise. $*$ is the convolution operator. We assume that n follows an i.i.d. Gaussian distribution with zero mean. We treat b, k, l, and n as vectors, i.e., b is a vector consisting of pixel values of a blurred image. Eq. (1) can be also expressed as:

$$b = Kl + n = Lk + n, \tag{2}$$

where K and L are convolution matrices corresponding to the blur kernel k and the latent image l, respectively.

2.2   Framework

Given that edge-based and power-spectrum-based methods have different advantages, combining them together seems to be a natural idea. However, doing it properly is not trivial. Directly combining the objective functions in both methods together may make the hybrid algorithm to perform worse than either one. That is because the salient edges and the power spectrum are only preferred by one method and may seriously deteriorate the other. In fact, both edge-based and power-spectrum-based methods have their own dedicated operations to remove the influence of undesired image information. For instance, bilateral and shock filterring are used in Cho and Lee's method [4] for removing small edges being considered for kernel estimation, and directional whitening has been used in Goldstein and Fattal's approach [11] for minimizing the influence of strong edges on computing the power spectrum. In this paper, we propose a framework that explicitly considers both the helpful and harmful image components of each method, so that the hybrid approach can perform better than each individual method.

The flowchart of the proposed hybrid approach is shown in Fig. 1. We adopt the widely-used multi-scale framework which has shown to be effective for kernel estimation, especially for edge-based methods [6, 7, 8, 9, 12]. In each scale, a latent image composed of only strong edges is predicted by image filtering operations as done in [4]. We use the same filtering operations and parameter settings to Cho and Lee's method
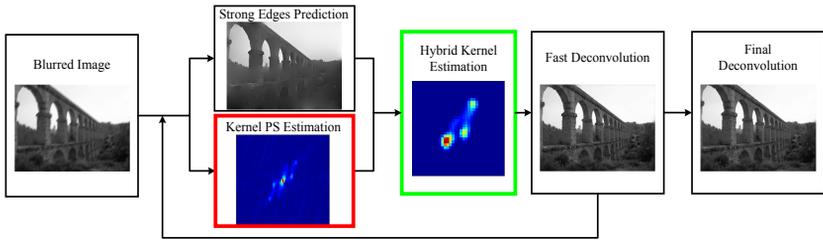
Fig. 1. The flowchart of the proposed hybrid deblurring method.

for this step. We refer the readers to [4] for details. The power spectrum of the kernel is estimated by compensating the initial power spectrum computed from the blurry image using the extracted edges in the latent image. The blur kernel is estimated then by optimizing a hybrid objective function that contains both edge and power spectrum terms. In each iteration, the latent image is computed fast by the deconvolution method with L_2 regularization term [4]. Finally, a state-of-the-art non-blind deconvolution algorithm with hyper-Laplacian priors [20] are applied to generate the final deblurred image.

In Sec. 3 and Sec. 4, we will describe the kernel power spectrum estimation and hybrid kernel estimation steps in more detail, which are our main technical contributions.

3   Kernel Power Spectrum Estimation

In this step, we estimate the power spectrum of the blur kernel from the input image, with the help of the current estimate of the latent image to reduce estimation errors caused by strong edges. The power spectrum estimated in this step will be used as a constraint in the blur kernel estimation process in Sec. 4.
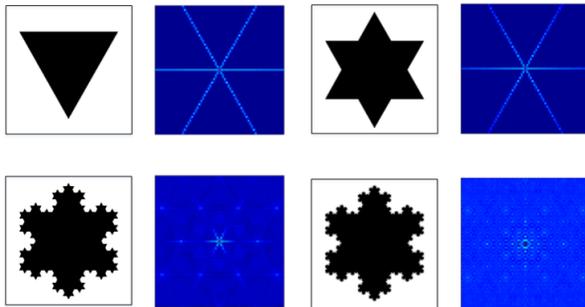
Fig. 2. The autocorrelation maps of Koch snowflake fractal images with 1st, 2nd, 4th and 6th iterations, from top-left to bottom-right, respectively. The edges with large gradient magnitude are regarded as good edges for edge-based methods. However, for spectrum based methods the straightness is more important. We can see that all the synthetic images have the same gradient magnitude, while they have totally different pattern in spectrum domain.

According to the power law of natural images [11], which assumes that natural images have fractal-like structures (as shown in Fig. 2), the power spectrum of a sharp image follows an exponential-like distribution. In other words, the autocorrelation of the gradient map of a natural sharp image can be approximated by a delta function:

$$(d * l) \otimes (d * l) \approx \delta, \tag{3}$$

where d is a derivative filter and $\otimes$ is the correlation operator. Given a blurry input image b, by adopting Eq. (1), we have:

$$(d * b) \otimes (d * b) = (d * (k * l + n)) \otimes (d * (k * l + n))$$
$$\approx k \otimes k * \delta + c_n \delta, \tag{4}$$

where c_n is the magnitude coefficient that can be computed as $c_n = 2\sigma_r^2$, and σ_r^2 is the variance of noise n. In the frequency domain, Eq. (4) becomes:

$$\mathcal{F}(d)\overline{\mathcal{F}(d)}\mathcal{F}(b)\overline{\mathcal{F}(b)} \approx |\mathcal{F}(k)|^2 + c_n, \tag{5}$$

where $\mathcal{F}(\cdot)$ denotes Fourier transform and $\overline{(\cdot)}$ is the complex conjugate. Therefore, the power spectrum of the blur kernel k can be approximated as:

$$|\mathcal{F}(k)| \approx \sqrt{\mathcal{F}(d)\overline{\mathcal{F}(d)}\mathcal{F}(b)\overline{\mathcal{F}(b)} - c_n}. \tag{6}$$

In practice, the power spectrum assumption in Eq. (3) may fail for images that contain strong edges (see Fig. 3(f)). On the other hand, not all strong edges will violate the assumption, and our observation is that only *straight lines* have a strong effect on it. To illustrate this finding, we show the autocorrelation maps of the gradients of Koch snowflake fractal images with different iterations in Fig. 2. It is obvious that the straight edges affect the power spectrum assumption significantly, and as the fractal grows the autocorrelation map follows the assumption better and better.

Therefore, to avoid bad effects from such straight lines, our method detects strong straight lines explicitly at each iteration, and remove the effect of them when computing the power spectrum. Specifically, we detect the straight lines from the current estimate of the latent image l using EDLine [21], and remove lines that are shorter than the blur kernel size. A dilation operation is applied on the detected line maps to generate a straight line mask.

Given the straight line mask, we can decompose the image l into two components as:

$$l = l_s + l_d, \tag{7}$$

where l_s is the structure component derive by masking l with the straight line mask, and l_d is the rest detail component. Eq. (4) then becomes:

$$(d * b) \otimes (d * b) \approx k \otimes k * ((d * l_s) \otimes (d * l_s) + c_d \delta) + c_n \delta, \tag{8}$$

where c_d is the magnitude coefficient of the detail component. Because the Fourier transform of impulse δ is a constant, c_d can be approximated as:

$$c_d = \frac{1}{N} \sum_{\omega_1, \omega_2} \mathcal{F}(d)\overline{\mathcal{F}(d)}\mathcal{F}(l_d)\overline{\mathcal{F}(l_d)}, \tag{9}$$
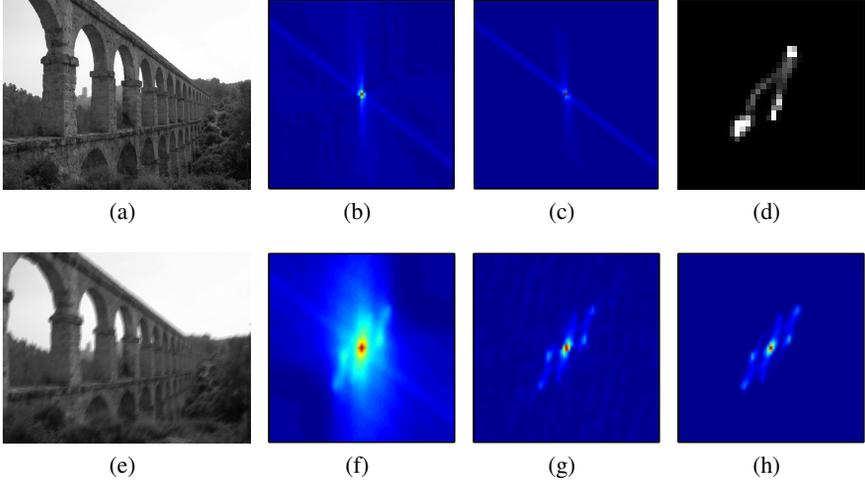
Fig. 3. Estimating the power spectrum of the blur kernel on a synthetic example. (a) latent image; (e) synthetically blurred input image; (b) power spectrum of (a); (f) power spectrum of kernel estimated from Eq. (6); (c) our estimated power-spectrum correction term (Denominator in Eq. 10); (g) corrected power spectrum map from Eq. (10); (d) the ground truth blur kernel; (h) the auto-correlation map of the ground truth kernel. Note that the corrected power spectrum in (g) is much closer to (h) compared with the original power spectrum in (f).

where (ω_1, ω_2) is the index of the 2D Fourier transform, and N is the number of elements in $\mathcal{F}(l_d)$. By applying Fourier transforms to Eq. (8), we can derive a new approximation for the power spectrum of the kernel K as:

$$|\mathcal{F}(k)| = \sqrt{\frac{\mathcal{F}(d)\overline{\mathcal{F}(d)}\mathcal{F}(b)\overline{\mathcal{F}(b)} - c_n}{\mathcal{F}(d)\overline{\mathcal{F}(d)}\mathcal{F}(l_s)\overline{\mathcal{F}(l_s)} + c_d}}. \qquad (10)$$

Fig. 3 shows an example of kernel power spectrum estimation on a synthetic example. It shows that the strong structural edges in the input image can significantly affect the power spectrum estimation, while our corrected power spectrum is much closer to the ground truth.

4   Hybrid Kernel Estimation

We now describe how to incorporate the estimated kernel power spectrum and the extracted strong edges into a unified framework for blur kernel estimation.

4.1   The formulation

Our optimization objective for kernel estimation contain a few terms. First, following previous work, we adopt a data term which is derived from the linear blur model in Eq. (1):

$$E_d(k) = \|p_x * k - b_x\|^2 + \|p_y * k - b_y\|^2, \qquad (11)$$

where p_x and p_y are gradient maps of latent sharp image, b_x and b_y are gradient maps of the input image b along the x and y directions, respectively.

Given the power spectrum information of the blur kernel, the magnitude of the Fourier transform of the blur kernel, which is equivalent to the power spectrum, can be constrained as:

$$E_s(k) = \||\mathcal{F}(k)| - |\mathcal{F}(k_s)|\|^2, \tag{12}$$

where $\mathcal{F}(k_s)$ is computed as in Eq. (10). Our energy function for kernel estimation then can be formulated as:

$$E(k) = E_d(k) + \alpha E_s(k) + \beta \|k\|_1 + \gamma \|\nabla k\|_2^2, \tag{13}$$

where α, β and γ are the weights for the power-spectrum-based, kernel sparsity and smoothness constraints respectively. In this paper, the weight of spectrum term α is set adaptively, and the rest parameters are set empirically by, $\beta = 150/(mn)$ and $\gamma = 0.2/max(m,n)$, where m, n are kernel size in x, y direction.

4.2 Optimization

To minimize the proposed energy function in Eq. (13), the phase retrieval problem need to be solved. Traditional phase retrieval algorithms [16, 17, 18] suffer from the well-known stagnation problem. Surprisingly, we found that a rough initialization of phase information provided by structural edges can greatly alleviate this problem. We empirically tested several phase retrieval methods, and found that even the simplest gradient descent method (error reduction) which has been shown to seriously suffer from stagnation can produce promising result in our framework. Therefore, we adopt this method for phase retrieval in our system.

Specifically, The gradient of the power-spectrum-based constraint term is derived as:

$$\frac{d\||\mathcal{F}(k)| - |\mathcal{F}(k_s)|\|^2}{dk} = 2(k - k'), \tag{14}$$

where

$$k' = \mathcal{F}^{-1}\left(|\mathcal{F}(k_s)|e^{i\theta}\right). \tag{15}$$

Here, $e^{i\theta}$ is the phase of the Fourier transform of the kernel k. For the detailed derivation, we refer the readers to [16]. The gradient of Eq. (13) becomes:

$$\begin{aligned}\frac{dE(k)}{dk} =& 2P_x^T P_x k + 2P_x^T P_x + \\ & 2P_y^T P_y k + 2P_y^T b_y + \\ & 2\alpha(k - k') + 2\beta W k + 2\gamma L k,\end{aligned} \tag{16}$$

where k is kernel in vector form, and L is Laplace operator, W is a diagonal matrix whose entries are defined by

$$W_{i,i} = \begin{cases} \frac{1}{k_i} & \text{if } k_i \neq 0 \\ 0 & \text{if } k_i = 0 \end{cases}, \tag{17}$$

where k_i is the i-th elements of kernel k. Finally, we set the descent direction g as $g = -dE(k)/dk$.

After determining the decent direction g, the optimal step length ζ is computed by minimizing Eq. (13) with respect to the step length ζ. Then, by finding the zero of $dE(k + \zeta g)/d\zeta$, we can derive the optimal ζ as:

$$\zeta = \frac{g^T g}{g^T \left(P_x^T P_x + P_y^T P_y + \alpha I + \beta W + \gamma L \right) g}. \tag{18}$$

In our implementation, the iterative procedure will be terminated when the update step size ζ is smaller than 10^{-7} or the iteration number is larger than 300.

4.3   Adaptive weighting

The weight α in Eqn. 13 is an important parameter that determines the relative importance of the power-spectrum-based term versus the edge-based ones. Ideally, it should be adaptively selected for a specific input image, based on which type of information can be extracted more reliably. The optimal weight thus depends on various factors of the input image, including the distributions and characteristics of the structural edges and textured regions, as well as the underlying blur kernel. However, given that we do not know the blur kernel beforehand, it is difficult to derive an analytic solution for determining the optimal α at the beginning of optimizing process. To alleviate this problem, we propose a machine learning approach to predict good α from low-level image features including both structure and texture descriptors. In particular, considering the characteristics of edge-based and spectrum-based methods, we extract the following two features:

1. Distributions of strong edges in different directions. We extract the straight line mask from the input image as described in Sec. 3, and compute the histogram of edge pixels in the extracted straight lines in different edge direction bins. In our implementation we divide the edge directions into 8 bins, resulting in a 8-dimensions vector that describes the richness of the strong edges that can be extracted from the input image. Intuitively, a balanced histogram usually means that strong edges exist in different directions, providing good constraints for solving the blur kernel reliably.
2. The richness of image details. We exclude the pixels inside the straight line mask and use the rest of pixels to compute a gradient magnitude histogram. This is under the consideration that if more pixels have large gradient magnitudes, then the input image probably contains rich texture details that are beneficial to the power-spectrum-based component. In our implementation we use a 8-bin histogram.

The complete feature vector for an input image thus have 16 dimensions. To train a regression model for predicting α, we used the 640-image dataset proposed by Sun *et al.* [9] as the training dataset, which contains the blurred input image and the ground truth latent image for each example. According to our experiments, the algorithm is not very sensitive for small changes of α. Thus, for each test image, we deblurred it using
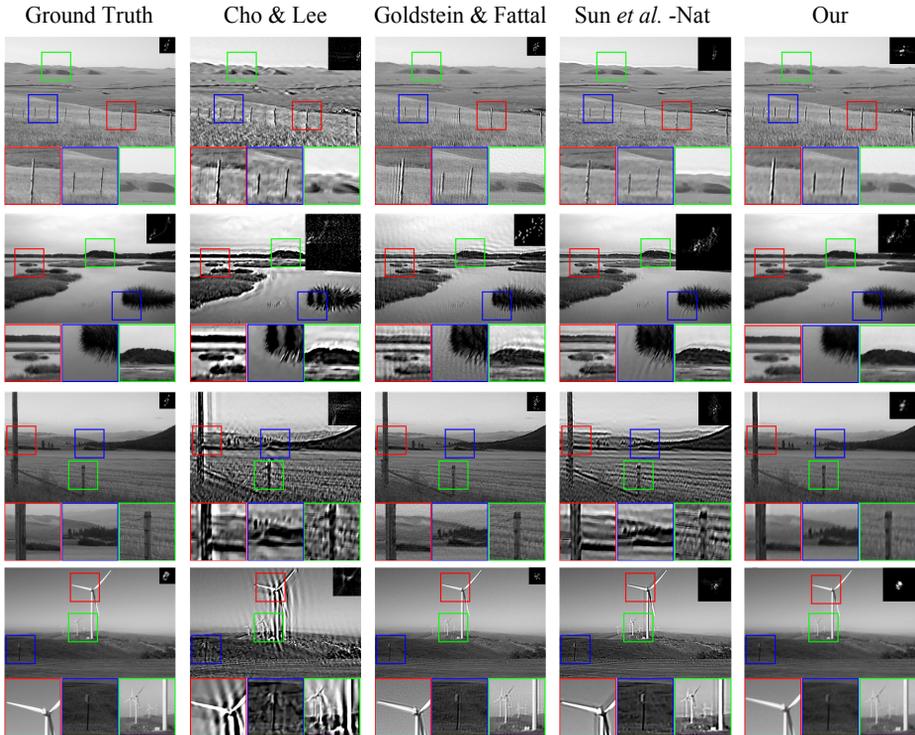
Fig. 4. Qualitative comparisons on four images from Sun *et al.*'s dataset [9]. From left to right: ground truth image and kernel, latent image and kernel estimated by Cho and Lee [4], Goldstein and Fattal [11], Sun *et al.* [9] and proposed method, respectively.

our method with 5 different settings of α: $\alpha = 0.1, 1, 10, 100, 1000$, and chose the one with the best deblurring quality as the target α value. In practice we found this discrete set of α weights can well represent the reasonable range of this parameter. We used the SVM as the classification model to label each input image with an α value. 480 images were randomly selected from the whole dataset for training and the remaining 160 images were used for testing. On the test dataset, the mean SSIM achieved by our method using the α weights predicted by the SVM model is 0.8195, while the mean SSIM achieved by using the ground truth α weights is 0.8241, just slightly higher than the trained model. This suggests that the proposed learning approach can effectively select good α values given an input blurry image.

5   Experiment Results

To evaluate the proposed method, we have applied it on both synthetic and real test datasets that have been proposed in previous work. We also compare our approach with state-of-the-art single image deblurring methods, both qualitatively and quantitatively.

Since our contribution is in the kernel estimation step, to ensure a fair comparison, we use Krishnan and Fergus's deconvolution method [20] to generate the final outputs for all kernel estimation approaches.

5.1   Comparisons on synthetic data

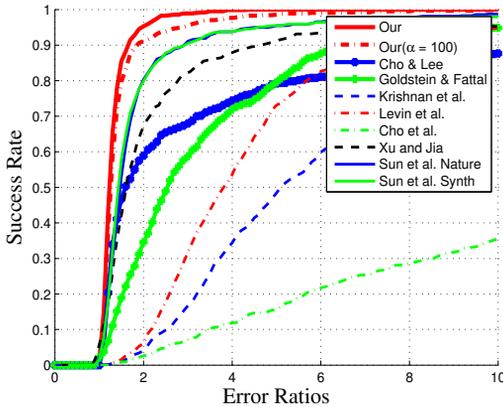We first apply our algorithm on some synthetic datasets that have been recently proposed.

Fig. 5. Success ratio vs. error ratio of our method and other algorithms on Sun *et al.*'s dataset [9].

Sun* et al.*'s dataset [9]. This dataset contains 640 images generated from 80 high quality nature images and 8 blur kernels. Fig. 4 shows some qualitative comparisons between our method and other state-of-the-art algorithms. It suggest that our methods achieves higher quality results than either edge-base (Cho and Lee [4] and Xu and Jia [12]) methods or power-spectrum-based (Goldstein and Fattal [11]) ones. Fig. 5 shows the cumulative distrutribution of error ratio metric (ratio between SSD errors of images deblurred from estimated and ground truth kenrels, see [22] for details) on this dataset, which also suggests that our method performs the best on this large scale dataset. We also tested our algorithm with different constant spectrum weights (α), and it achieved the best performance when $\alpha = 100$ on this dataset, which is better than previous algorithms, but still worse than using adaptive weights proposed in Sec. 4.3.

Levin* et al.*'s dataset [22]. This dataset has 32 images generated from 4 small size images (255×255 pixels) and 8 blur kernels (kernels' supports varys from 10∼25 pixels). All the kernels estimated by Cho and Lee [4], Goldstein and Fattal [11] and proposed methods are shown in Fig. 6(a)(b)(c) respectively. Notice that the power-spectrum-based method does not perform well on this dataset, as some of the kernels shown in Fig. 6(b) contain large errors. This is because the corresponding images in this dataset do not contain enough image texture for reliable kernel estimation. Our hybrid method correctly handles this situation, and generates results that are mostly similar but slightly better to those of the edge-based method [4].
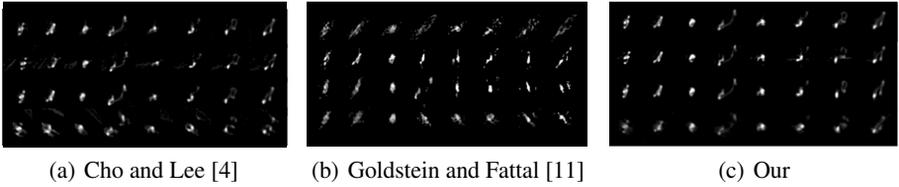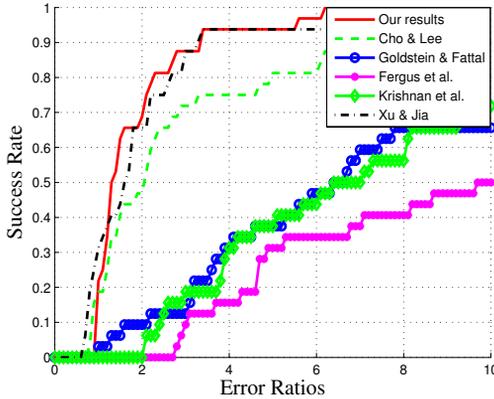
(a) Cho and Lee [4]   (b) Goldstein and Fattal [11]   (c) Our

Fig. 6. Kernels estimated by by Cho and Lee [4], Goldstein and Fattal [11] and proposed methods on Levin *et al.*'s dataset [22].

Fig. 7. Error ratios of different methods on Levin *et al.*'s dataset [22].

Fig. 7 shows the cumulative distributions of error ratio on this dataset. Note that the success rates in this plot are lower than those in the original plot [22]. This is because we found that since the kernel sizes are relatively large with respect to the image sizes in this dataset, the border artifacts are serious, and the SSD error mainly occurs in the border region. To eliminate the influence of border artifacts introduced by deconvolution methods, we cut off the border region in the error ratio calculation.

As shown in Eq. (13), our hybrid method contains edge-based terms that are similar to those in Cho and Lee's method [4], and a power spectrum term similar to the one in Goldstein and Fattal's method [11]. The hybrid method performs better than both individual methods on this dataset, showing the advantage of this fusion strategy.

Image without strong edges. To better understand the effectiveness of the spectrum component of the proposed method, we apply it on a texture image shown in Fig. 9(a,b). The results estimated by Cho and Lee [4], Goldstein and Fattal [11] and our method are shown in Fig. 9(c), (d) and (e), respectively. It is not a surprise that the edge-based method (Cho and Lee [4]) completely fails on this image, since it contains no strong edges. On the other hand, both Goldstein and Fattal [11] and our method produce good results given that the blur kernel can be well extracted from the power spectrum information.
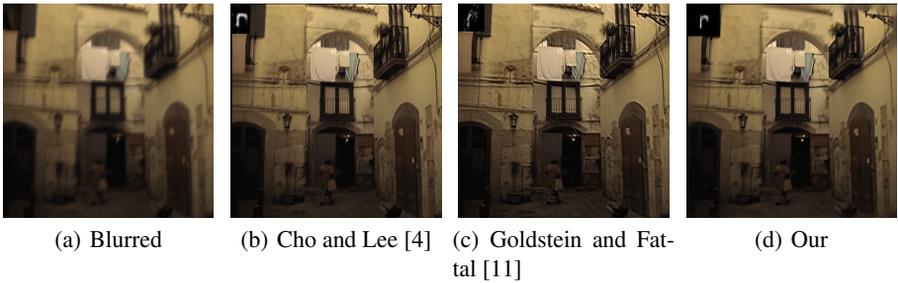
| (a) Blurred | (b) Cho and Lee [4] | (c) Goldstein and Fattal [11] | (d) Our |

Fig. 8. Qualitative Comparisons of one image from dataset [23].

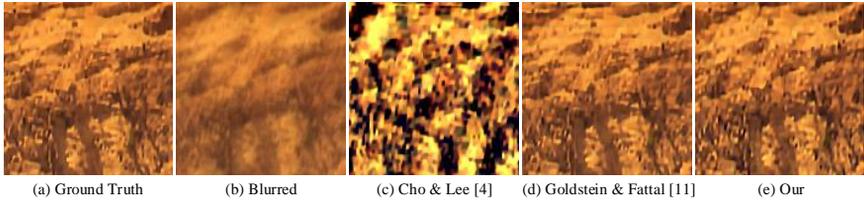| (a) Ground Truth | (b) Blurred | (c) Cho & Lee [4] | (d) Goldstein & Fattal [11] | (e) Our |

Fig. 9. Performance of proposed algorithm on the image without strong edges.

5.2 Comparisons on real examples

Non-uniform dataset from Köhler et al. *[23].* This dataset contains real blurry images systematically generated from 4 sharp image and 12 non-uniform kernels. The quantitative comparison results on this dataset is shown in Table. 1. It suggests that the proposed method consistently achieves better performance than the state-of-the-art image deblurring algorithms, including uniform and non-uniform, edge-based and spectrum-based methods.

In this dataset, the spectrum-based method [11] performs much worse than other methods. This is because the stagnate and robustness problem of the phase retrieval algorithm is much more severe when the blur kernel is large. Because our algorithm can take advantage of the phase information estimated from structural image edges, the

Table 1. Quantative comparsion on Köhler *et al.*'s dataset [23]

| Methods	Image 01		Image 02		Image 03		Image 04		Total	
	PSNR	SSIM	PSNR	SSIM	PSNR	SSIM	PSNR	SSIM	PSNR	SSIM
Whyte *et al.* [24]	27.5475	0.7359	22.8696	0.6796	28.6112	0.7484	24.7065	0.6982	25.9337	0.7155
Hirsch *et al.* [25]	26.7232	0.7513	22.5867	0.7290	26.4155	0.7405	23.5364	0.7060	24.8155	0.7317
Shan *et al.* [6]	26.4253	0.7001	20.5950	0.5872	25.8819	0.6920	22.3954	0.6486	23.8244	0.6570
Fergus *et al.* [14]	22.7770	0.6858	14.9354	0.5431	22.9687	0.7153	14.9084	0.5540	18.8974	0.6246
Krishnan *et al.* [7]	26.8654	0.7632	21.7551	0.7044	26.6443	0.7768	22.8701	0.6820	24.5337	0.7337
Goldstein & Fattal [11]	25.9454	0.7024	21.3887	0.6836	24.2768	0.6989	23.3397	0.6820	23.7377	0.6917
Cho & Lee [4]	28.9093	0.8156	24.2727	0.8008	29.1973	0.8067	26.6064	0.8117	27.2464	0.8087
Xu & Jia [12]	29.4054	0.8207	**25.4793**	0.8045	29.3040	0.8162	26.7601	0.7967	27.7372	0.8095
Our	**30.1340**	**0.8819**	25.4749	**0.8439**	**30.1777**	**0.8740**	**26.7661**	**0.8117**	**28.1158**	**0.8484**
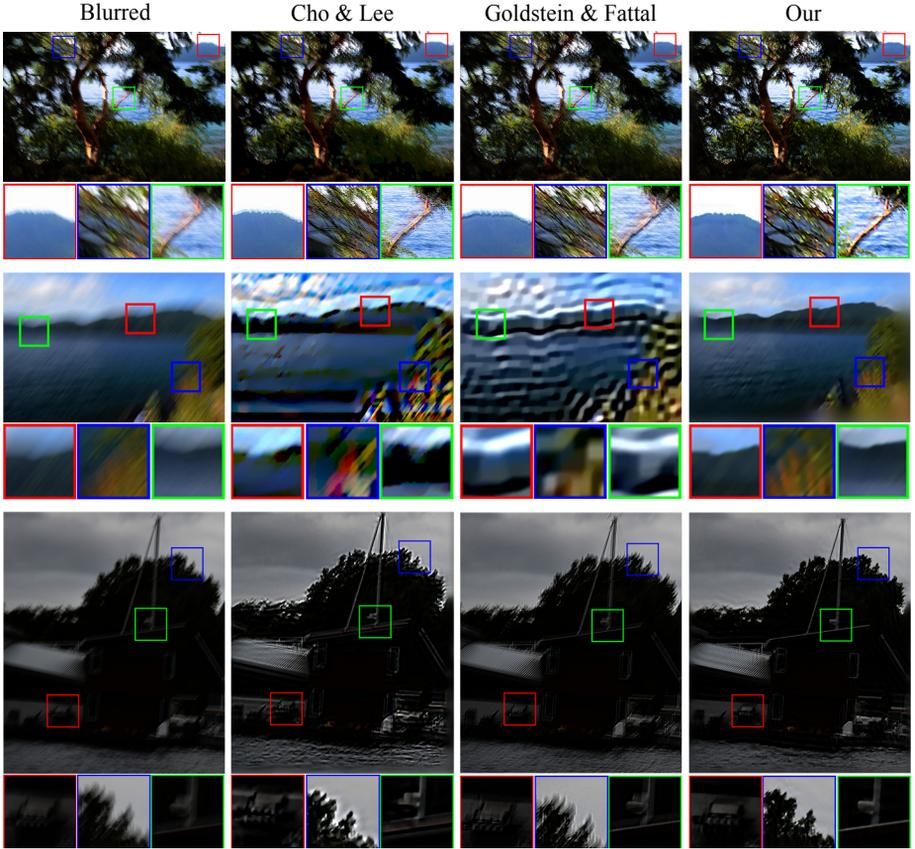
Fig. 10. Comparisons on real-world examples.

phase retrieval algorithm works much better in our method, which in turn improves the performance of the hybrid kernel estimation.

  Real-world examples. Fig. 10 shows three real-world blurry images with unknown blur parameters, and the deblurring results of Cho and Lee [4], Goldstein and Fattal [11] and the proposed approach. It suggest that previous edge-based and power-spectrum-based methods cannot achieve satisfactory results on these examples. In contrast, our approach is able to generate much higher quality results on these examples.

5.3   The contribution of the two priors

One may wonder how much contribution each prior has in the hybrid approach. Given that most natural images contain some amount of sharp or strong edges, edge information is more universal, thus the edge prior plays a more dominant role in determining the blur kernel. Our approach reveals that the true merit of the power-spectrum prior is its ability to augment edge-based information. When edge-based methods fail badly,

(a) Blurred   (b) Cho and Lee [4]   (c) Whyte *et al.* [24]   (d) Our results
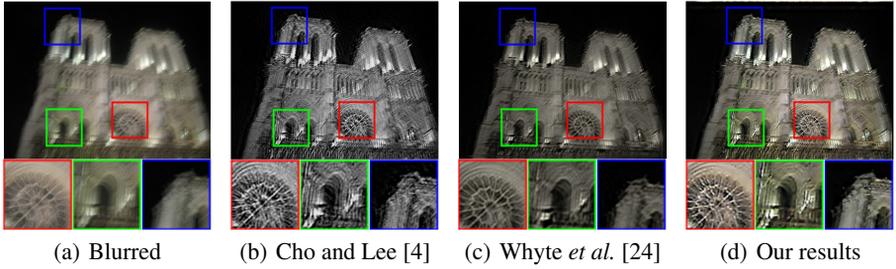
Fig. 11. Comparisons on an image with significant non-uniform blur.

such as the examples in the 3rd and 4th rows of Fig. 4, power-spectrum prior leads to significant improvements. In these examples, although strong edges exist, they concentrate in few directions, making kernel estimation ill-posed. The complementary information from the power spectrum makes kernel estimation possible in these cases. In other cases where edge-based methods generate reasonable results, incorporating the power-spectrum prior further improves the kernel accuracy and leads to higher quality results. To demonstrate this we conducted additional experiments by setting alpha=0 (meaning no power-spectrum at all), and the quantitative results are significantly worse in all data sets (e.g. 2.7dB worse on dataset of [9]).

5.4   Limitation

The main limitation of the proposed approach is that it cannot handle significant non-uniform blur well, because the power spectrum prior is based on global statistics that does not consider spatially-varying blur. In Fig. 11 we apply our algorithm on one of the images that contain significant non-uniform blur in Whyte *et al.*'s dataset [24]. It shows that the result generated by our method (Fig. 11(d)) is worse than that of the non-uniform deblurring algorithm (Fig. 11(c)), and is comparable to Cho and Lee's result (Fig. 11(b)). This suggests that the power spectrum term does not help when dealing with non-uniform blur.

6   Conclusion

We propose a new hybrid deblurring approach that restores blurry images by the aid of both edge-based and power-spectrum-based priors. Our approach extracts the strong edges from the image, and use them for estimating a more accurate power spectrum of the kernel. Both the edges and the improved power spectrum of the blur kernel are then combined in an optimization framework for kernel estimation. Experimental results show that our method achieves better performance than either edge-based or power-spectrum-based methods.

References

1. Jia, J.: Single Image Motion Deblurring Using Transparency. In: CVPR. (2007)
2. Joshi, N., Szeliski, R., Kriegman, D.J.: PSF estimation using sharp edge prediction. In: CVPR. (2008)
3. Money, J.H., Kang, S.H.: Total variation minimizing blind deconvolution with shock filter reference. Image and Vision Computing **26**(2) (February 2008) 302–314
4. Cho, S., Lee, S.: Fast motion deblurring. ACM Transactions on Graphics **28**(5) (December 2009) 1
5. Cho, T.S., Paris, S., Horn, B.K.P., Freeman, W.T.: Blur kernel estimation using the radon transform. In: CVPR. (2011)
6. Shan, Q., Jia, J., Agarwala, A.: High-quality motion deblurring from a single image. ACM Transactions on Graphics **27**(3) (August 2008) 1
7. Krishnan, D., Tay, T., Fergus, R.: Blind deconvolution using a normalized sparsity measure. In: CVPR. (2011)
8. Xu, L., Zheng, S., Jia, J.: Unnatural L 0 Sparse Representation for Natural Image Deblurring. In: CVPR. (2013)
9. Sun, L., Cho, S., Wang, J., Hays, J.: Edge-based blur kernel estimation using patch priors. In: ICCP. (2013)
10. Hu, W., Xue, J.: PSF Estimation via Gradient Domain Correlation. IEEE Trans. on Image Process **21**(1) (2012) 386–392
11. Goldstein, A., Fattal, R.: Blur-Kernel Estimation from Spectral. In: ECCV. (2012)
12. Xu, L., Jia, J.: Two-phase kernel estimation for robust motion deblurring. In: ECCV. (2010)
13. Zhong, L., Cho, S., Metaxas, D., Paris, S., Wang, J.: Handling Noise in Single Image Deblurring using Directional Filters. In: CVPR. (2013)
14. Fergus, R., Singh, B., Hertzmann, A., Roweis, S.T., Freeman, W.T.: Removing camera shake from a single photograph. ACM Transactions on Graphics **25**(3) (July 2006) 787
15. Yitzhaky, Y., Mor, I., Lantzman, A., Kopeika, N.S.: Direct method for restoration of motion-blurred images. JOSA A **15**(6) (2000) 1512–1519
16. Fienup, J.R.: Phase retrieval algorithms: a comparison. Applied optics **21**(15) (August 1982) 2758–69
17. Fienup, J., Wackerman, C.: Phase-retrieval stagnation problems and solutions. JOSA A **3**(11) (1986) 1897–1907
18. Luke, D.R.: Relaxed averaged alternating reflections for diffraction imaging. Inverse Problems **21**(1) (February 2005) 37–50
19. Osherovich, E.: Numerical methods for phase retrieval. PhD thesis
20. Krishnan, D., Fergus, R.: Fast Image Deconvolution using Hyper-Laplacian Priors. In: NIPS. (2009)
21. Akinlar, C., Topal, C.: EDLines: A real-time line segment detector with a false detection control. Pattern Recognition Letters **32**(13) (October 2011) 1633–1642
22. Levin, A., Weiss, Y., Durand, F., Freeman, W.: Understanding and evaluating blind deconvolution algorithms. In: CVPR. (2009)
23. Köhler, R., Hirsch, M., Mohler, B., Schölkopf, B., Harmeling, S.: Recording and playback of camera shake : benchmarking blind deconvolution. In: ECCV. (2012) 255
24. Whyte, O., Sivic, J., Zisserman, A., Ponce, J.: Non-uniform deblurring for shaken images. International journal of computer … (2012)
25. Hirsch, M., Schuler, C., Harmeling, S., Schölkopf, B.: Fast removal of non-uniform camera shake. In: ICCV. (2011)